NANO LETTERS

Letter

pubs.acs.org/NanoLett

Ultrathin Two-Dimensional Atomic Crystals as Stable Interfacial Layer for Improvement of Lithium Metal Anode

Kai Yan,[†] Hyun-Wook Lee,[†] Teng Gao,[⊥] Guangyuan Zheng,[‡] Hongbin Yao,[†] Haotian Wang,[§] Zhenda Lu,[†] Yu Zhou,[⊥] Zheng Liang,[†] Zhongfan Liu,[⊥] Steven Chu,[∥] and Yi Cui*[,†,#]

[†]Department of Materials Science and Engineering, [‡]Department of Chemical Engineering, [§]Department of Applied Physics, and [∥]Department of Physics, Stanford University, Stanford, California 94305 United States

[⊥]Center for Nanochemistry, Beijing National Laboratory for Molecular Sciences (BNLMS), State Key Laboratory for Structural Chemistry of Unstable and Stable Species, College of Chemistry and Molecular Engineering, Peking University, Beijing 100871, People's Republic of China

[#]Stanford Institute for Materials and Energy Sciences, SLAC National Accelerator Laboratory, 2575 Sand Hill Road, Menlo Park, California 94025, United States

S *Supporting Information*

ABSTRACT: Stable cycling of lithium metal anode is challenging due to the dendritic lithium formation and high chemical reactivity of lithium with electrolyte and nearly all the materials. Here, we demonstrate a promising novel electrode design by growing two-dimensional (2D) atomic crystal layers including hexagonal boron nitride (h-BN) and graphene directly on Cu metal current collectors. Lithium ions were able to penetrate through the point and line defects of the 2D layers during the electrochemical deposition, leading to sandwiched lithium metal between ultrathin 2D layers and Cu. The 2D layers afford an excellent interfacial protection of Li metal due to their remarkable chemical stability as well as mechanical strength and flexibility, resulting from the strong intralayer bonds and ultrathin thickness. Smooth Li metal deposition without dendritic and mossy Li formation was realized. We showed stable cycling over 50 cycles with Coulombic efficiency ~97% in organic carbonate electrolyte with current density and areal capacity up to the practical value of 2.0 mA/cm^{2}and 5.0 mAh/cm^2, respectively, which is a significant improvement over the unprotected electrodes in the same electrolyte.

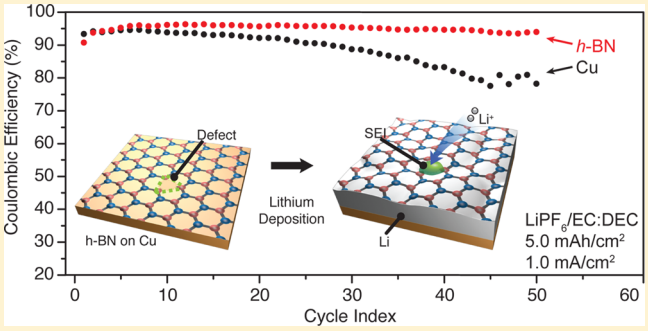

KEYWORDS: *Lithium metal anode, Coulombic efficiency, boron nitride, graphene*

Lithium ion batteries have been a great success as the power source for portable electronics.[1,2] The emerging applications in electric vehicles have stimulated research on high-energy battery chemistry such as Si anodes,[3,4] Li–S, and Li–air.[5] Li metal anode has the highest specific capacity of 3860 mAh/g of Li and the lowest anode potential and has long been considered as the "Holy Grail" in lithium-based batteries. However, the problems of dendritic and mossy Li formation and its highly reactive nature cause poor safety and low cycling efficiency during charge/discharge, preventing lithium metal anode from wide applications.[6,7] Four decades of research to study Li metal plating/stripping process[8−12] and to address the problems by electrolyte additives[13−17] and solid polymer and ceramics coating[18−21] have increased our understanding but not yet solved the problems.

The challenges of Li metal anodes are fundamentally rooted to two reasons. The first one is mechanical in nature. During battery charge and discharge, Li metal plating and striping process take place without a host material. Different from the host nature of graphite[22] and Si anodes[3,4] in lithium ion batteries that confine lithium ions inside, the spatial control of Li deposition in Li metal anodes is absent, resulting in various possible morphologies including dangerous dendrites. Compared with the finite volume expansion of graphite (~10%) and silicon (~400%) anode hosts, the "hostless" Li metal has virtually infinite relative volumetric change. Such a drastic volume change creates significant mechanical instability and cracks in electrodes and their interfaces. The second reason is chemical. Li metal reacts with nearly all the chemical species in gas, liquid, and solid phases. In liquid electrolyte, Li metal decomposes solvent and salts to form solid–electrolyte interphase (SEI).[23] There is very little control over the SEI thickness, grain size, chemical composition, or spatial distribution of the reaction products.[6] Such an SEI layer is weak against the unavoidable mechanical deformation during Li plating/striping and it continuously breaks and repairs by

Received: August 14, 2014
Revised: August 24, 2014

   dx.doi.org/10.1021/nl503125u | *Nano Lett.* XXXX, XXX, XXX–XXX

reacting with more electrolyte. At the breaking point without adequate or timely repair, Li dendrite can grow out and be further amplified by strong local flux of lithium ions. These processes together cause the challenges of dendritic and mossy lithium formation, low Coulombic efficiency, and short cycle life (Figure 1a).

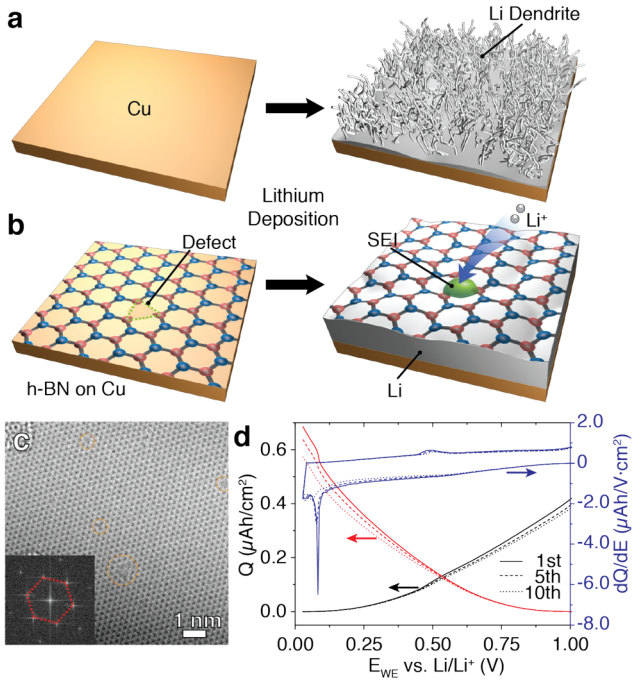

Figure 1. Schematic diagrams of lithium deposition and characterizations of h-BN film. (a) Deposition of Li metal on bare copper substrate. A large number of Li dendrites would grow because the lack of confinement. Spontaneously formed SEI layer with certain weak spots triggers ramified growth of lithium dendrite, resulting in significant consumption of electrolyte as well as safety issues. (b) The subnanometer defects in h-BN film grown on copper serve as channels for Li ions during lithium deposition. Lithium is deposited between h-BN and copper. The stiff B−N bond and chemical stability prevent dendrite formation and lithium corrosion, respectively. (c) HR-TEM image of monolayer h-BN film with hexagonal lattice. Triangular point defects clearly observed as indicated by orange triangles. Inset: FFT of TEM image shows a single set of hexagonal spot pattern. (d) Capacity and differential capacity versus potential of galvanostatic cycling of h-BN coated Cu foil at current density of 10 $\mu A/cm^2$.

In the past, studies on electrolyte additives are aimed to form the SEI layers with improved stability and therefore to suppress the further reaction with electrolyte and dendrite formation.[13−17] However, the thus formed SEI layers have limited mechanical strength and are still broken during Li metal plating/striping and cannot provide the desirable functions. A recent self-healing electrostatic shield mechanism was proposed with alkaline ion additives to suppress dendrite growth yet continued reaction with electrolyte is not avoidable shown by the low Coulombic efficiency of 76.6%.[17] Another strategy utilizing rigid polymer and ceramic layers as solid electrolyte to suppress Li dendrite growth has resulted in notable progress[18−21] although their low ionic conductivity at room and low temperature, large thickness, high interfacial impedance, and chemical instability against Li metal remain as concerns. Development of fast lithium ion conductor such as such as $Li_{10}GeP_2S_{12}$ and garnet type $Li_7La_3Zr_2O_{12}$,[20,24] could offer a promise along this direction yet to be developed. In addition, novel strategy that regulates lithium deposition with insulating layer was recently proved to promote the performance of lithium metal,[25] though the improvement is limited.

Built on the past literature studies and our own understanding on Li metal, we believe that the hostless deposition of Li metal needs to be controlled with materials both chemically stable and mechanically strong. We propose a novel electrode structure with thin layers of such materials covering the Cu current collector and hope that the Li metal deposition/striping takes place between (Figure 1b). Recently, we demonstrated a promising interfacial nanomaterial approach based on hollow carbon nanospheres,[26] although we believe that novel interfacial materials with even higher chemical stability and mechanical strength are still urgently needed, especially for more corrosive electrolyte such as organic carbonate. When searching for materials with such properties, we look into two-dimensional atomic crystal layer materials including graphene and h-BN, which have been intensely studied for electronics, sensors, supercapacitors, and electromechanical devices.[27−31] Both graphene and h-BN have the following attractive properties for our purpose: (1) They are known to be chemically inert and stable against most chemicals including Li metal. (2) Their single atomic layers have very strong mechanical strength, resulted from strong intralayer bonding. The in-plane elastic stiffness of single atomic layer corresponds to Young's modulus approaching 1.0 TPa for both graphene and h-BN.[32,33] That is more than two-order magnitude higher than that of Li metal (4.9 GPa) and also much higher than those common inorganic components in native SEI (Li_2CO_3 68 GPa, LiF 65 GPa, Li_2O 141 GPa). Graphene and h-BN are in principle strong enough to sustain the pressure induced by the growth of lithium metal dendrite. (3) The pore diameter within each hexagonal ring for graphene and h-BN is only ∼1.4 and ∼1.2 Å, respectively. These numbers are smaller than the diameter of Li^+ ions (∼1.8 Å) and Li atoms (∼2.7 Å) and much smaller than any molecules in electrolyte. Therefore, no chemical species can diffuse through the layers and Li metal cannot move through the ring pore, either. Indeed, the past studies showed that even helium (0.6 Å diameter) cannot penetrate the graphene sheet.[34] On the other hand, the point and line defects are known within chemically grown 2D layers and allow the penetration of small ions including Li^+ in solution with the ionic permeability proportional to the size and density of defects.[35,36] For example, with one boron atom missing the diameter of defect formed by three nitrogen atoms after relaxation would be ∼3.11 Å,[37] which is just enough for the penetration of lithium ion. In addition, these subnanometer-sized defects surrounded by dangling bonds could be easily sealed by ionic conducting SEI, creating an ideal channel allowing the exchange of lithium ions but blocking both the penetration of lithium metal and the diffusion of electrolyte molecules. (4) Despite the large in-plane strength, 1−10 layers of graphene and h-BN are highly flexible due to their ultrathin thickness (from sub-1 nm to sub-10 nm). Their high flexibility can be important to accommodate the Li metal deposition. The difference between graphene and h-BN is that graphene is a semimetal and h-BN is an insulator with a large bandgap of 5.9 eV. We start our concept demonstration by first using h-BN because direct Li metal deposition on h-BN is likely to be prohibited due to its insulating nature.

We used the method of chemical vapor deposition (CVD) developed recently for synthesis of large-area h-BN.[38,39] Similar

dx.doi.org/10.1021/nl503125u | Nano Lett. XXXX, XXX, XXX−XXX

with the CVD growth of graphene, copper foil was heated up to 1000 °C in argon and hydrogen at low pressure followed by ammonia borane (NH_3−BH_3) vapor (see methods in Supporting Information for details). The partial pressure of precursor was kept at ∼100 mTorr for up to 10 min. At the initial stage of growth, discrete triangles of h-BN domains ∼2 μm in edge were found (Supporting Information Figure S1b−d). These grains gradually grow and connect with each other and coalescent into a continuous film with line defects along grain boundaries.[40] Within 10 min, multilayered h-BN films can form and cover the whole copper substrate with a crack hardly visible. Recent studies suggested that the grain boundary may be sealed by the adlayers during the growth of 2D material.[41] Therefore, the h-BN film is expected to be strongly reinforced with increased thickness due to reduced grain boundaries. The h-BN films are flexible but mechanically strong enough to be self-supported with dimension up to millimeters, as shown in Supporting Information Figure S2e. The thickness of the film was determined to vary from 1 to 10 atomic layers depending on the growth time and pressure with layer distance of 0.35 ± 0.02 nm (Supporting Information Figure S2f), matching with the crystal structure of h-BN.[37] High-resolution transmission electron microscopy (HR-TEM) image in Figure 1c shows atomically resolved hexagonal lattice of single layer h-BN, indicating the nature of atomic crystals. The fast Fourier transform (FFT) pattern in the inset of Figure 1c gives a lattice distance of 0.249 nm, corresponding well to the B−N bond length.[37] It is noticeable that vast point defects exist within the h-BN plane (shown by the orange circles in Figure 1c). According to the TEM image, the average distance between defects is estimated to be ∼2 nm, which corresponds to a defect density in the order of 10^{13} cm^{-2}. These point defects, together with line defects at grain boundaries, serve as active channels for lithium ions during the electrochemical cycling of lithium metal anode.

The h-BN film is further confirmed by Raman spectroscopy and X-ray photoemission spectroscopy (XPS). A prominent peak at 1369 cm^{-1} in the Raman spectrum taken on a few-layered h-BN film corresponds to the B−N vibration mode (E_{2g}) within basal plane of h-BN (Supporting Information Figure S2d).[42] Two sharp peaks located at 190.3 and 397.9 eV in XPS spectrum matches the exact binding energy of B 1s and N 1s electrons in B−N bond, respectively (Supporting Information Figure S2b,c).[43] In addition, the ratio of B/N was found to be 1:1.04, which is consistent with the stoichiometry of h-BN.

The as-grown h-BN samples with adequate thickness (6−10 layers) on copper were directly used to build batteries with Li metal as counter electrodes. We used carbonate-based electrolyte (1 M $LiPF_6$ in ethylene carbonate (EC)/diethyl carbonate (DEC)), which are widely used in the existing lithium ion batteries (LIBs). Comparing with ether electrolyte, the performance of Li metal cycling in carbonate-based electrolyte is rather poor with low Coulombic efficiency because of its relatively positive electrochemical window and the poor mechanical strength of its native SEI layer.[44] There is a great value if we can make this common electrolyte to work for Li metal anodes.

We first cycled the BN protected Cu foil electrode from 0.01 to 1.0 V against lithium at low current density of 10 μA/cm^2. Surprisingly, a short plateau appeared around 80 and 500 mV during reduction and oxidation, respectively (Figure 1d). The plateau was further confirmed in the differential capacity curve, where prominent peaks were observed at the specific potential. The plateau was found to be reproducible in more than 10 cycles. Considering the superior insulating property of h-BN, we ascribe the plateaus to the insertion and extraction of lithium ions between h-BN layer and Cu substrate, which allowed lithium plating and stripping in the gap thereafter. In addition, the areal capacity contributed by h-BN prior to lithium plating was found to be less than 1 μAh/cm^2, which is three magnitudes lower than the capacity of lithium metal we would demonstrate in this work.

Lithium metal was plated to the Cu substrate galvanostatically afterward. For the bare copper anode, the cross-sectional scanning electron microscopy (SEM) images (Figure 2a) show that wire-shaped Li dendrites and mossy Li with diameter 1−2 μm already form after first deposition of 1.0 mAh/cm^2 lithium at current rate of 0.5 mA/cm^2. The surface area of dendritic Li is increased drastically, consuming much electrolyte to form SEI. For the h-BN/Cu electrodes, the cross-sectional SEM images (Figure 2c) show large size pancake-like Li metal covered by h-BN film. The top surface of Li pancakes seems to be flat. The situation is rather similar when we use solution exfoliated h-BN flakes instead. We found that Li grains could be well capped underneath the h-BN flake after electrochemical deposition (Supporting Information Figure S4). The surface area is significantly smaller than that on the bare Cu electrode, therefore consuming much less electrolyte. More importantly, with the protection of h-BN most of the lithium surface is isolated from direct contact with electrolyte. Comparing top view SEM images (Figure 2e,f for bare Cu and Figure 2g,h for h-BN/Cu, respectively), we can clearly see the rough and grainy surface for the bare Cu electrodes, reflecting the top of many dendrites but the flat and smooth top surface for the h-BN/Cu electrodes. The typical pancake size in the h-BN/Cu electrodes is around 5−10 μm. It appears that the h-BN layers are sitting on top of Li pancakes. That is, Li metal is sandwiched between h-BN and Cu, further reducing the surface area exposed to the electrolyte. In fact, the successful encapsulation of lithium can significantly suppress lithium reaction with oxygen and moisture in the air (Supporting Information Figure S5). We cannot completely exclude yet the possibility of the SEI formation at the boundaries of h-BN patches, where part of Li metal surface might be still exposed to the electrolyte. However, we expect that the exposed Li surface area is reduced dramatically. On the basis of these results, we present the schematic electrode structure for the bare-Cu and the h-BN/Cu electrodes as shown in Figure 2b,d, respectively. The h-BN sheets serve as stable interfacial layers for Li metal deposition.

The morphology of Li after 10 cycles of galvanostatic plating and stripping with current rate of 0.5 mA/cm^2 was also studied. For the bare Cu, the SEI layer is broken and repaired repeatedly during the cycling, resulting in serious nonuniformity within the layer. Consequently, dendrites with even sharper tips grew from the weak spots of the SEI layer (Figure 2i,j). With feature size of only several hundreds nanometers, these thin dendrites not only contribute an even larger surface area than the first deposition, as well as a higher possibility of dead lithium upon stripping, but also potentially threat the safety of batteries by penetrating through the separator. For the situation with h-BN protection, the surface of anode is still very smooth but seems to have some SEI mixing h-BN (Figure 2k,l). The mixture of h-BN and genuine SEI from electrolyte reaction serves as a complex film covering lithium grains. This complex film is

dx.doi.org/10.1021/nl503125u | Nano Lett. XXXX, XXX, XXX−XXX

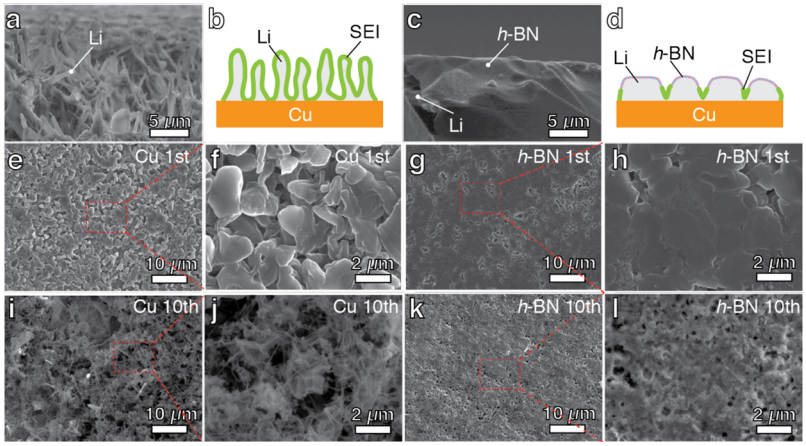

Figure 2. Morphology studies of Li metal deposition. (a) Cross section SEM image of deposited Li metal on bare copper. (b) Schematic structure of Li metal deposited on copper. (c) Cross section SEM image of deposited Li metal protected by h-BN. (d) Schematic structure of Li metal with h-BN protection. Li metal might be exposed to electrolyte between patches of h-BN film, resulting in the SEI formation. (e,f) Top view SEM images of the first lithium deposition on bare copper with current rate of 0.5 mA/cm^2. (g,h) Top view SEM images of the first lithium deposition on h-BN protected anode with the same condition. (i,j) Top view SEM images of the 10th lithium deposition on bare copper with current rate of 0.5 mA/cm^2. (k,l) Top view SEM images of the 10th lithium deposition with h-BN protection with the same condition.

expected to stabilize the surface of lithium with good mechanical strength and ionic conductivity. No Li dendrite was found, however, over the whole anode surface, indicating the successful suppression of Li dendrite growth by top-capping h-BN layers.

The cycling Coulombic efficiencies of bare copper and h-BN protected copper were further examined in organic carbonate electrolyte with Li foil as counter electrode. The areal capacity for each lithium deposition was fixed at 1.0 mAh/cm^2 followed by the extraction of Li, while the current rate varied from 0.2 to 2.0 mA/cm^2. The Coulombic efficiency is calculated as the ratio of the extraction versus the deposition capacity. The value of Coulombic efficiency is crucial for practical lithium metal anode, because it not only describes how much capacity can be recovered, but also indicates how much electrolyte is consumed to build SEI upon every cycle. Despite the counter Li foil with virtually infinite amount of Li, limiting the deposition capacity of Li on working electrodes allows us to evaluate the meaningful Coulombic efficiency of working electrode. This is different from many previous studies where the meaningful Coulombic efficiency cannot be obtained. For current density of 0.5 mA/cm^2 (Figure 3a), the Coulombic efficiency of on bare copper started at 95% and drops quickly to only 80% in less than 50 cycles. This fast decaying process on bare Cu is consistent with the evolutionally increased surface area and reaction with electrolyte of lithium dendrites. Excitingly, the situation with h-BN is totally different. The Coulombic efficiency of lithium cycling on h-BN protected anode is 87% for the first cycle, where there might be certain trapping of lithium under h-BN layer and at the edge sites of grain boundaries. The efficiency quickly rose up to approximately 97% and remained stable for more than 50 cycles. This result outperformed the control battery with vinyl carbonate as an additive on bare Cu[15] (Supporting Information Figure S6). The improvement in Coulombic efficiency indicates the reduced reaction between lithium metal and electrolyte, therefore suggesting that the complex layer of SEI and h-BN is more stable than the SEI layer alone.

When the current density is increased to a practically relevant value of 1.0 mA/cm^2, the performance for bare copper became even worse. The Coulombic efficiency decayed to below 80% in less than 30 cycles with serious fluctuation attributed to the large surface morphology change and electrolyte consumption at high current density. In comparison, the Coulombic efficiency of the h-BN/Cu electrodes remains high and stable above 95% for more than 50 cycles. The significant improvement in Coulombic efficiency strongly suggests the effect of h-BN film in protecting lithium metal anode from reacting with electrolyte. We note that despite improvement such a Coulombic efficiency is still not yet adequate for long cycle life in full battery cells, calling for future study such as combining h-BN with additives.

A concern on having h-BN covering the Cu surface is that the h-BN might block the Li^+ ion flux during plating and stripping. In order to address this issue, we measured the voltage profile during the cell charge/discharge with different current density. The difference (hysteresis) between charge and discharge voltages would reflect the kinetics loss due to ion flux. As shown in Figure 3d, the voltage profiles for the cycling of lithium on the two kinds of electrodes at current rate of 0.5 mA/cm^2 coincide well at the potential of lithium plating and stripping. The voltage hystereses of the two types of electrodes over 50 cycles for two current rates (0.5 and 1 mA/cm^2, Figure 3a) are nearly identical. These results have two implications. First, they confirm that there is not much reduction of Li^+ ion flux by covering Cu with h-BN. The ionic diffusion through atomic defects and edges of h-BN is adequate to maintain the high flux of Li+ ions. Second, they also provide evidence to exclude the possibility that deposition of lithium took place on top of h-BN, which would require a much higher voltage for the tunneling of electrons through h-BN film.

The Coulombic efficiency and voltage hysteresis averaged over 25 cycles at different current densities is summarized in Figure 3c. The significant improvement in cycling efficiency by h-BN is clear over all current density. The voltage hysteresis is nearly identical for the two types of electrodes. As expected, they all increase with current density. It can be concluded that h-BN is capable of protecting Li metal anode at various current rate.

dx.doi.org/10.1021/nl503125u | *Nano Lett.* XXXX, XXX, XXX−XXX

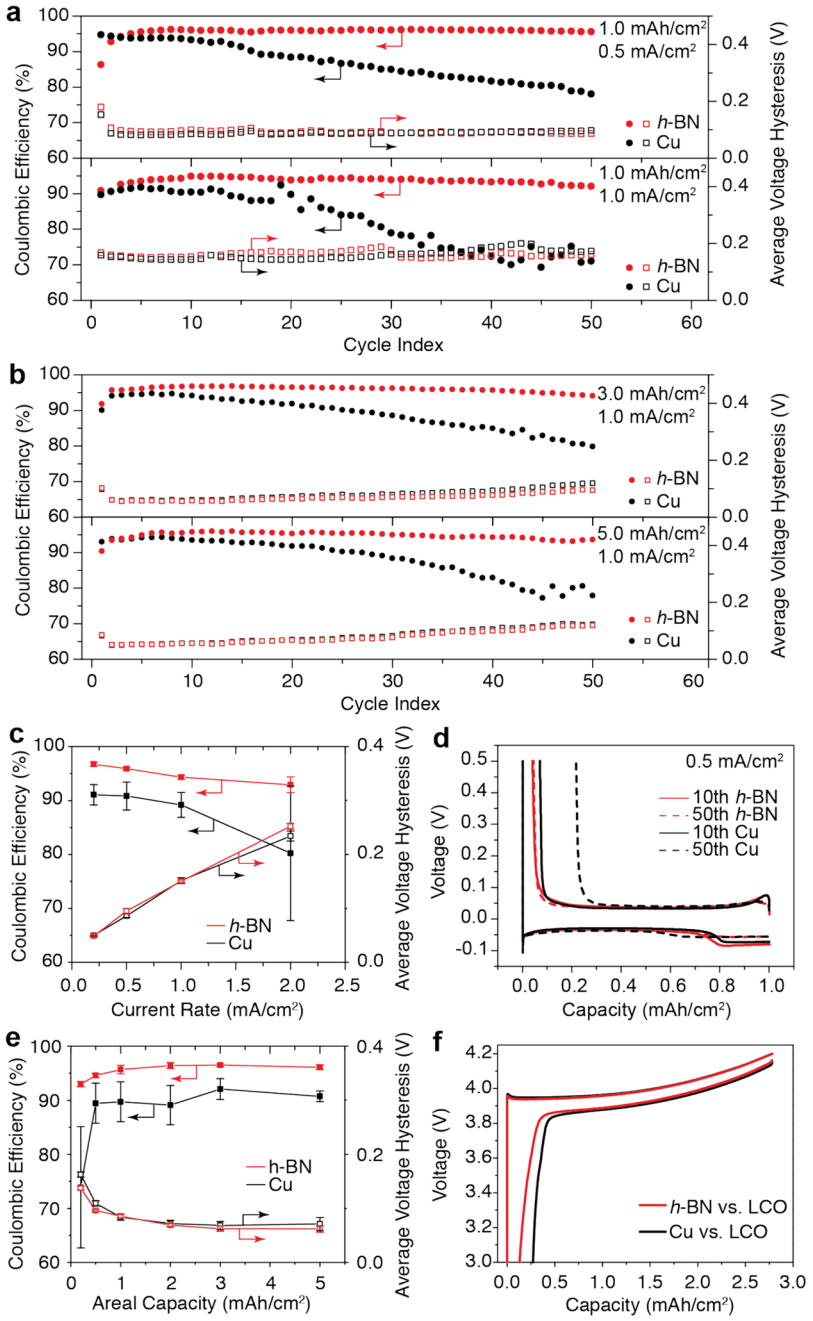

Figure 3. Cycling performance of Li metal anode with h-BN protection at various current rates. (a) Coulombic efficiency and voltage hysteresis of Li anode with and without h-BN protection at current rate of 0.5 and 1.0 mA/cm^2. (b) Coulombic efficiency and voltage hysteresis of Li anode with and without h-BN protection at different areal capacity of 3.0 and 5.0 mAh/cm^2. (c) Statistics on cycling efficiency and average voltage hysteresis from 6th to 30th cycle of Li metal anode at different current rate from 0.2 to 2.0 mA/cm^2 with 1.0 mAh/cm^2 areal capacity. (d) Voltage profile of 10th and 50th cycle with and without h-BN protection. (e) Statistics on cycling efficiency and average voltage hysteresis from 6th to 30th cycle of lithium metal anode with different areal capacity from 0.2 to 5.0 mAh/cm^2 at 0.5 mA/cm^2 current rate. (f) Voltage profile of full cell with lithium cobalt oxide as cathode and empty copper foil with and without h-BN protection as anode.

One the other hand, the performance of lithium batteries at elevated temperature is always a big concern because increased side reactions would quickly deteriorate batteries. For bare Cu substrate, we found the Coulombic efficiency is reduced by more than 5% when the battery is cycled at 50 °C. Comparatively, the electrode covered with h-BN exhibited little decrease in Coulombic efficiency as shown in Supporting Information Figure S7, indicating that highly inert h-BN could still afford effective protection of Li metal at high temperature.

For the practical batteries, areal capacities >3 mAh/cm^2 are needed. The unique working mechanism of h-BN in principle allow for effective protection of Li film with different thickness, because the whole layer is always on top of the Li layer during operation. In order to prove the concept, we explored the dependence of Coulombic efficiency as a function of areal capacity (0.2, 0.5, 1.0, 2.0, 3.0, 5.0 mAh/cm^2) at constant current rate of 0.5 mA/cm^2 (Supporting Information Figure S8). Figure 3b shows the results on high practical areal capacities of 3.0 and 5.0 mAh/cm^2 with current density of 1.0

dx.doi.org/10.1021/nl503125u | Nano Lett. XXXX, XXX, XXX−XXX

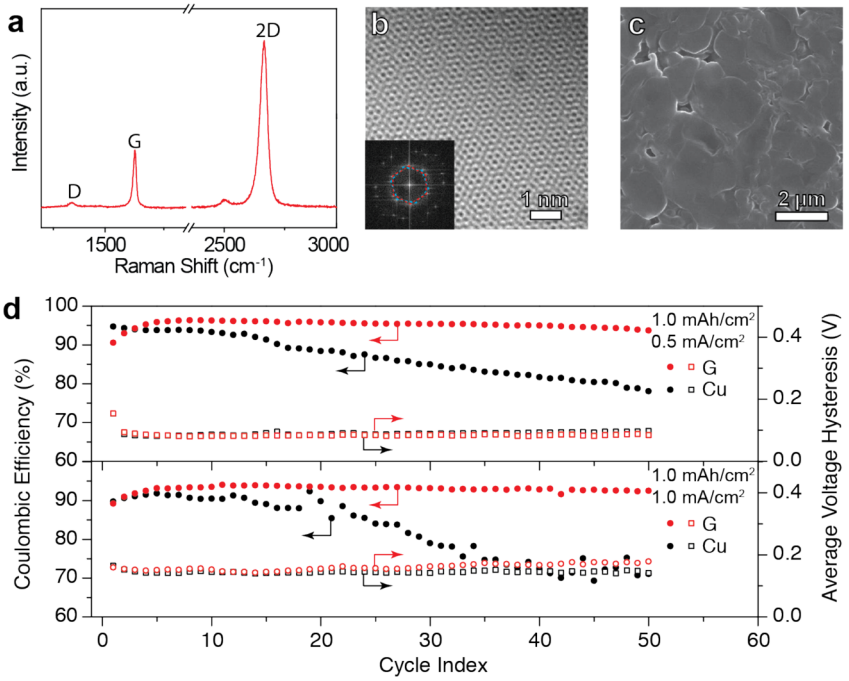

Figure 4. Characterizations of graphene and its performance in cycling of Li metal anode. (a) Raman spectrum of graphene film. The wavelength of excitation laser is 632.8 nm. (b) HR-TEM image of mismatched two-layer graphene. Two sets of hexagonal spot patterns were shown in the FFT image inset. (c) Top view SEM image of the first Li metal deposition on graphene protected anode at 0.5 mA/cm^2. (d) Cycling performance and average voltage hysteresis of Li metal anode with and without graphene protection at different current rate.

mA/cm^2. The Coulombic efficiency of h-BN/Cu electrodes remains high at 95−97% even at these high areal capacities, which are much higher and more stable than the bare Cu electrodes that decays from 92 to 80%. Figure 3e summarizes the averaged Coulombic efficiency versus areal capacity. The h-BN/Cu electrodes are consistently much better than the bare electrodes for all the areal capacity. For both types of electrodes, the Coulombic efficiency shows noticeable drop for the low areal capacity (<0.5 mAh/cm^2). This may arise from the constant amount of electrolyte reaction from the top of electrodes regardless of lithium thickness. For small areal capacity, this amount accounts for a large fraction.

The capability of h-BN protection for lithium metal anode up to a practical areal capacity opens up the opportunity to construct full batteries with, for example, lithium cobalt oxide ($LiCoO_2$) as cathode. As a demonstration, full batteries were built with $LiCoO_2$ as cathode and current collector only as "empty anode". Figure 3f shows the voltage versus the areal capacity of the full cell composed of two types of empty anodes (bare Cu and h-BN/Cu) at current density of 0.5 mA/cm^2, the h-BN/Cu cells show 10% more discharge capacity than the bare Cu cells for the same charge capacity of 2.8 mAh/cm^2. Despite the significant improvement with h-BN, the Coulombic efficiency is still not high enough yet for long-term cycling of full cell with empty anode. Further improvement to >99.5% will be carried out in our future research with electrolyte additives and systematic tuning of h-BN layers.

The concept of protecting lithium with inert atomic thin layers could also be extended to graphene. The CVD-grown graphene of high quality on Cu was confirmed by a weak D band and sharp G and 2D bands in Raman spectrum (Figure 4a).[45] The HR-TEM image of two mismatched graphene layers in Figure 4b demonstrates the highly crystallized two-dimensional hexagon frameworks.[46] The length of C−C bond was calculated from the FFT pattern as ∼0.141 nm, which is consistent with the reported value of graphene. Even though graphene is generally regarded as a semimetal with extra-ordinary carrier mobility, the interlayer conductivity is quite limited.[47] It is also known that electron transfer from the graphene basal plane to outside is sluggish. In addition, any electron transfer can result in the formation of SEI first on graphene basal plane above the Li metal deposition potential. It is thus reasonable to expect that just like the h-BN/Cu electrode, Li metal deposition would take place between graphene and Cu but not on top of graphene. Figure 4c shows the top surface of graphene/Cu electrodes after lithium deposition with comparable smoothness to that of h-BN, confirming the same deposition behavior. With the protection of graphene film, the cycling performance of lithium metal anode shows significant improvement over the bare Cu electrodes. The graphene/Cu anodes exhibit high Coulombic efficiency of ∼95 and ∼93% over 50 stable cycles at current rate of 0.5 and 1.0 mA/cm^2 with areal capacity of 1.0 mAh/cm^2, respectively (Figure 4d). Compared to h-BN, the improvement of Coulombic efficiency is less, which might arise from the smaller average thickness of graphene in our CVD growth.[45] The conductive nature of graphene may also contribute partially considering the possible deposition at active edges.

In conclusion, our work introduces two-dimensional atomic crystal layered materials including h-BN and graphene as an effective protective layer to form the 2D layer−Li−Cu sandwich structure, which effectively suppresses the dendrites and mossy lithium formation and improves the cycling efficiency by reducing the reaction with electrolyte. The unique protective mechanism of two-dimensional materials allows for protection of lithium with various areal capacities at different current rates. Such a protection is confirmed not to introduce diffusion barrier for Li ions.

dx.doi.org/10.1021/nl503125u | *Nano Lett.* XXXX, XXX, XXX−XXX

■ ASSOCIATED CONTENT

Supporting Information

Details about materials synthesis and characterizations, testing battery assembly and electrochemical measurements, additional SEM images of lithium metal deposition on different substrates, electrochemical cycling performance of batteries with vinyl carbonate additive and at elevated temperature, respectively. This material is available free of charge via the Internet at http://pubs.acs.org.

■ AUTHOR INFORMATION

Corresponding Author

*E-mail: yicui@stanford.edu.

Notes

The authors declare no competing financial interest.

■ ACKNOWLEDGMENTS

This work was supported by the Assistant Secretary for Energy Efficiency and Renewable Energy, Office of Vehicle Technologies of the U.S. Department of Energy. G.Z. acknowledges financial support from Agency for Science, Technology and Research (A*STAR), Singapore. H.-W.L. was supported by Basic Science Research Program through the National Research Foundation of Korea under Contract No. NRF-2012R1A6A3A03038593.

■ REFERENCES

(1) Tarascon, J. M.; Armand, M. *Nature* **2001**, *414*, 359.
(2) Chu, S.; Majumdar, A. *Nature* **2012**, *488*, 294.
(3) Chan, C. K.; Peng, H.; Liu, G.; McIlwrath, K.; Zhang, X. F.; Huggins, R. a.; Cui, Y. *Nat. Nanotechnol.* **2008**, *3*, 31.
(4) Wu, H.; Chan, G.; Choi, J. W.; Ryu, I.; Yao, Y.; McDowell, M. T.; Lee, S. W.; Jackson, A.; Yang, Y.; Hu, L.; Cui, Y. *Nat. Nanotechnol.* **2012**, *7*, 310.
(5) Bruce, P. G.; Freunberger, S. A.; Hardwick, L. J.; Tarascon, J.-M. *Nat. Mater.* **2012**, *11*, 19.
(6) Aurbach, D.; Zinigrad, E.; Cohen, Y.; Teller, H. *Solid State Ionics* **2002**, *148*, 405.
(7) Xu, W.; Wang, J.; Ding, F.; Chen, X.; Nasybulin, E.; Zhang, Y.; Zhang, J.-G. *Energy Environ. Sci.* **2014**, *7*, 513.
(8) Aurbach, D.; Cohen, Y. *J. Electrochem. Soc.* **1996**, *143*, 3525.
(9) Gireaud, L.; Grugeon, S.; Laruelle, S.; Yrieix, B.; Tarascon, J. M. *Electrochem. Commun.* **2006**, *8*, 1639.
(10) Bhattacharyya, R.; Key, B.; Chen, H.; Best, A. S.; Hollenkamp, A. F.; Grey, C. P. *Nat. Mater.* **2010**, *9*, 504.
(11) Chandrashekar, S.; Trease, N. M.; Chang, H. J.; Du, L.-S.; Grey, C. P.; Jerschow, A. *Nat. Mater.* **2012**, *11*, 311.
(12) Harry, K. J.; Hallinan, D. T.; Parkinson, D. Y.; Macdowell, A. A.; Balsara, N. P. *Nat. Mater.* **2014**, *13*, 69.
(13) Hirai, T.; Yoshimatsu, I.; Yamaki, J. *J. Electrochem. Soc.* **1994**, *141*, 2300.
(14) Shiraishi, S.; Kanamura, K.; Takehara, Z. *J. Electrochem. Soc.* **1999**, *146*, 1633.
(15) Ota, H.; Shima, K.; Ue, M.; Yamaki, J. *Electrochim. Acta* **2004**, *49*, 565.
(16) Lee, Y. M.; Seo, J. E.; Lee, Y.-G.; Lee, S. H.; Cho, K. Y.; Park, J.-K. *Electrochem. Solid State Lett.* **2007**, *10*, A216.
(17) Ding, F.; Xu, W.; Graff, G. L.; Zhang, J.; Sushko, M. L.; Chen, X.; Shao, Y.; Engelhard, M. H.; Nie, Z.; Xiao, J.; Liu, X.; Sushko, P. V.; Liu, J.; Zhang, J.-G. *J. Am. Chem. Soc.* **2013**, *135*, 4450.
(18) Croce, F.; Appetecchi, G. B.; Persi, L.; Scrosati, B. *Nature* **1998**, *394*, 456.
(19) Nimon, Y. S.; Chu, M.-Y.; Visco, S. J. *Coated lithium electrodes.* US6537701 B1, 2003.
(20) Kamaya, N.; Homma, K.; Yamakawa, Y.; Hirayama, M.; Kanno, R.; Yonemura, M.; Kamiyama, T.; Kato, Y.; Hama, S.; Kawamoto, K.; Mitsui, A. *Nat. Mater.* **2011**, *10*, 682.
(21) Bouchet, R.; Maria, S.; Meziane, R.; Aboulaich, A.; Lienafa, L.; Bonnet, J. P.; Phan, T. N. T.; Bertin, D.; Gigmes, D.; Devaux, D.; Denoyel, R.; Armand, M. *Nat. Mater.* **2013**, *12*, 452.
(22) Dahn, J. R.; Zheng, T.; Liu, Y.; Xue, J. S. *Science* **1995**, *270*, 590.
(23) Peled, E. *J. Electrochem. Soc.* **1979**, *126*, 2047.
(24) Murugan, R.; Thangadurai, V.; Weppner, W. *Angew. Chem., Int. Ed.* **2007**, *46*, 7778.
(25) Ji, X.; Liu, D.-Y.; Prendiville, D. G.; Zhang, Y.; Liu, X.; Stucky, G. D. *Nano Today* **2012**, *7*, 10.
(26) Zheng, G.; Lee, S. W.; Liang, Z.; Lee, H.-W.; Yan, K.; Yao, H.; Wang, H.; Li, W.; Chu, S.; Cui, Y. *Nat. Nanotechnol.* **2014**, *9*, 618.
(27) Novoselov, K. S.; Geim, a. K.; Morozov, S. V.; Jiang, D.; Zhang, Y.; Dubonos, S. V.; Grigorieva, I. V.; Firsov, a. a. *Science* **2004**, *306*, 666.
(28) Shao, Y.; Wang, J.; Wu, H.; Liu, J.; Aksay, I. A.; Lin, Y. *Electroanalysis* **2010**, *22*, 1027.
(29) Zhu, Y.; Murali, S.; Stoller, M. D.; Ganesh, K. J.; Cai, W.; Ferreira, P. J.; Pirkle, A.; Wallace, R. M.; Cychosz, K. A.; Thommes, M.; Su, D.; Stach, E. A.; Ruoff, R. S. *Science* **2011**, *332*, 1537.
(30) Zhang, Y.; Tan, Y.; Stormer, H. L.; Kim, P. *Nature* **2005**, *438*, 201.
(31) El-Kady, M. F.; Strong, V.; Dubin, S.; Kaner, R. B. *Science* **2012**, *335*, 1326.
(32) Lee, C.; Wei, X.; Kysar, J. W.; Hone, J. *Science* **2008**, *321*, 385.
(33) Kudin, K. N.; Scuseria, G. E.; Yakobson, B. I. *Phys. Rev. B* **2001**, *64*, 235406.
(34) Bunch, J. S.; Verbridge, S. S.; Alden, J. S.; van der Zande, A. M.; Parpia, J. M.; Craighead, H. G.; McEuen, P. L.; Zande, A. M. V. D. *Nano Lett.* **2008**, *8*, 2458.
(35) Garaj, S.; Hubbard, W.; Reina, A.; Kong, J.; Branton, D.; Golovchenko, J. a. *Nature* **2010**, *467*, 190.
(36) O'Hern, S. C.; Boutilier, M. S. H.; Idrobo, J.-C.; Song, Y.; Kong, J.; Laoui, T.; Atieh, M.; Karnik, R. *Nano Lett.* **2014**, *14*, 1234.
(37) Jin, C.; Lin, F.; Suenaga, K.; Iijima, S. *Phys. Rev. Lett.* **2009**, *102*, 195505.
(38) Song, L.; Ci, L.; Lu, H.; Sorokin, P. B.; Jin, C.; Ni, J.; Kvashnin, A. G.; Kvashnin, D. G.; Lou, J.; Yakobson, B. I.; Ajayan, P. M. *Nano Lett.* **2010**, *10*, 3209.
(39) Kim, K. K.; Hsu, A.; Jia, X. T.; Kim, S. M.; Shi, Y. S.; Hofmann, M.; Nezich, D.; Rodriguez-Nieva, J. F.; Dresselhaus, M.; Palacios, T.; Kong, J. *Nano Lett.* **2012**, *12*, 161.
(40) Gibb, A. L.; Alem, N.; Chen, J.-H.; Erickson, K. J.; Ciston, J.; Gautam, A.; Linck, M.; Zettl, A. *J. Am. Chem. Soc.* **2013**, *135*, 6758.
(41) Kim, S. M.; Hsu, A.; Araujo, P. T.; Lee, Y.-H.; Palacios, T.; Dresselhaus, M. S.; Idrobo, J.-C.; Kim, K. K.; Kong, J. *Nano Lett.* **2013**, 933.
(42) Geick, R.; Perry, C. H.; Rupprech, G. *Phys. Rev.* **1966**, *146*, 543.
(43) Trehan, R. *J. Vac. Sci. Technol., A* **1990**, *8*, 4026.
(44) Aurbach, D. *Nonaqueous electrochemistry*; Marcel Dekker: New York, 1999; p viii, 602.
(45) Li, X.; Cai, W.; An, J.; Kim, S.; Nah, J.; Yang, D.; Piner, R.; Velamakanni, A.; Jung, I.; Tutuc, E.; Banerjee, S. K.; Colombo, L.; Ruoff, R. S. *Science* **2009**, *324*, 1312.
(46) Meyer, J. C.; Geim, A. K.; Katsnelson, M. I.; Novoselov, K. S.; Booth, T. J.; Roth, S. *Nature* **2007**, *446*, 60.
(47) Primak, W. *Phys. Rev.* **1956**, *103*, 544.